J Solid State Electrochem (2012) 16:3383–3390
DOI 10.1007/s10008-012-1784-6

ORIGINAL PAPER

Influence of annealing temperature on microstructural and electrochemical properties of rf-sputtered $LiMn_2O_4$ film cathodes

K. Jayanth-Babu · P. Jeevan-Kumar · O. M. Hussain · C. M. Julien

Received: 19 January 2012 / Revised: 19 May 2012 / Accepted: 23 May 2012 / Published online: 8 June 2012

Abstract The microstructural and electrochemical properties of rf-sputtered $LiMn_2O_4$ films were investigated as a function of post-deposition process. The degree of crystallization in the films gradually increased with the increase of annealing temperature (T_a). The films annealed at T_a=973 K exhibited characteristic peaks with predominant (111) orientation representing the cubic spinel structure of *Fd3m* symmetry. The estimated Mn–Mn and Mn–O distances obtained from the X-ray diffraction data were observed to be increased slightly with T_a. Characteristic changes in surface morphological features were observed as a function of T_a as evidenced from scanning electron microscopy. The estimated root mean square (RMS) roughness of the films increased from 97 to 161 nm with augmentation of T_a. The electrochemical studies, viz. cyclic voltammetry (CV), specific discharge capacity and Li ion diffusion coefficient were carried out for annealed $LiMn_2O_4$ films in saturated aqueous electrolyte (Li_2SO_4) in the potential window of 0–1.2 V and correlated with surface morphology and grain size. The $LiMn_2O_4$ films annealed at T_a=973 K exhibited better electrochemical performance and demonstrated a discharge capacity of about 53.5 μA h cm^{-2} μm^{-1} with diffusion coefficient of 1.2×10^{-13} cm^2 s^{-1}.

K. Jayanth-Babu · P. Jeevan-Kumar · O. M. Hussain (✉)
Thin Film Laboratory, Department of Physics,
Sri Venkateswara University,
Tirupati 517 502, India
e-mail: hussainsvu@gmail.com

C. M. Julien
Physicochimie des Electrolytes Colloïdes et Sciences Analytiques,
UMR 7195, Université Pierre et Marie Curie,
4 place Jussieu,
75005 Paris, France

Keywords $LiMn_2O_4$ thin films · rf sputtering · Annealing · Microstructure · Electrochemical properties

Introduction

Lithium manganese oxide ($LiMn_2O_4$) with the spinel structure is one of the most extensively studied cathode material for Li/Li^+ rechargeable batteries due to its low cost, non-toxicity and comprises relatively high energy density of 148 mA h g^{-1} [1, 2]. It crystallizes in normal cubic structure, in which the Li^+ and $Mn^{3+/4+}$ ions occupy the 8*a* tetrahedral and 16*d* octahedral sites, respectively, of cubic close packed oxygen array to give a cation distribution of $[Li]_{8a}[Mn]_{16d}O_4$. A strong edge shared octahedral $[Mn_2]O_4$ array permits reversible extraction of the Li^+ ions from the tetrahedral sites without collapsing the three dimensional $[Mn_2]O_4$ spinel frame work [3, 4]. The $Li_xMn_2O_4$ provides relatively high voltage (4 V) in the region of $0<x<1$ and a plateau at 3 V in the $1<x<2$ region. In the high voltage region, it exhibits two step reversible de-intercalation and intercalation of lithium mechanism. In the first step, lithium is inserted and de-inserted in a single phase region of spinel ($0.5<x<1.0$), while in the second step a phase transformation from spinel to a λ-MnO_2 occurs in the range ($0.0<x<0.5$) [5]. However, its application is limited due to significant capacity fading rate with cycle number. Several factors such as dissolution of the $Li_xMn_2O_4$ electrode in the electrolyte (as Mn^{2+}), structural instability due to the Jahn–Teller distortion and instability of organic based electrolyte in high voltage region [6, 7].

It has been observed that the $LiMn_2O_4$ in thin-film form shown better cycling stability than its powder counter parts and can be effectively used as binder free cathode material in the fabrication of all solid state microbatteries [8]. However because of the complex nature of $LiMn_2O_4$, deposition

of stoichiometric and single phase spinel structured films with good adhesion is a challenging problem. The value of cubic lattice parameter, which is directly related to the average oxidation state of the manganese, is crucial to obtain the effective cycling. Thin films of $LiMn_2O_4$ have been prepared by several physical and chemical vapour deposition techniques [9–13]. Among these techniques, the rf-magnetron sputtering technique is observed to be one of the most favorable and industrially viable techniques since it enables the formation of homogeneous films with definite thickness along with good adhesion. Also the microstructural properties can be altered by properly controlling the deposition parameters. Therefore numerous researchers were extensively studied the $LiMn_2O_4$ thin films by rf-magnetron sputtering technique [13–16]. In general, it is well acquaint that $LiMn_2O_4$ thin films annealed at higher temperatures exhibits better electrochemical property due to (1) increase of surface roughness, (2) increase of grain size and (3) enhancement of the stability of the host matrix of $LiMn_2O_4$, which favors Li-ion kinetics. $LiMn_2O_4$ thin films grown or annealed at higher temperatures always show preferred orientation providing high rate of Li diffusivity [11]. Annealing at elevated temperatures may enhance the grain size and surface area which has the key participation in the improvement of electrochemical activity of thin film cathodes [17]. Therefore, better understanding of the film surface properties in correlation with the electrochemical properties becomes the most significant study and also attracted many researchers due to growing interest in designing the portable electronic power sources. Nevertheless, the significance of $LiMn_2O_4$ in thin film form as positive cathode in advance Li-ion batteries shows impetus scope to carry out the research to investigate microstructural and electrochemical performance in presence of aqueous electrolyte.

The study of electrochemical performance in aqueous electrolyte has several advantages over non-aqueous electrolytes which includes low cost and greater safety [18]. In addition, the ionic conductivity of aqueous electrolyte is generally greater than the organic electrolyte [19] allowing higher rates and low voltage drops due to low electrolyte impedance. Li et al. [20] and coworkers used synthesized $LiMn_2O_4$ powders as cathode material to construct aqueous rechargeable coin-type lithium batteries and were first reported. Also, most of the investigators studied the electrochemical properties of $LiMn_2O_4$ thin-film electrodes in organic electrolyte cells (non-aqueous electrolyte) [21] but meager research reports are available with aqueous electrolyte solutions [22].

In the present investigation, $LiMn_2O_4$ films (LMOFs) are deposited on metallized silicon substrates by using rf-magnetron sputtering technique at a moderate substrate temperature. The films are subjected for annealing in controlled oxygen environment subsequently at various temperatures (T_a) and studied in detail the influence of microstructural properties. Structural characterization includes X-ray diffraction (XRD) and scanning electron microscopy (SEM). Investigation of the electrochemical activity of the $LiMn_2O_4$ thin films as positive electrodes is made in aqueous electrolyte solution that it is an alternate inexpensive electrochemical characterization tool to evolve the properties of thin film materials.

Experimental details

$LiMn_2O_4$ films about 0.8 μm thick were deposited from a 3-in.-diameter cold-pressed and sintered lithium-rich $LiMn_2O_4$ target using rf-magnetron sputtering technique onto Si/SiO_2 (0.3 μm)/Ti(0.03 μm)/Au(0.3 μm) substrate. The system was evacuated to a base pressure of less than 5×10^{-7} mbar with a turbo-molecular pumping system backed by a rotary pump. The distance between the target and the substrate was maintained constant at 5.0 cm. During the deposition, the substrate temperature T_s was kept at 523 K and the sputtered gas (O_2/Ar) composition was maintained at 1:6 to minimize the loss of lithium. The rf power applied to the target was 80 W and the pressure inside the chamber was about 2×10^{-2} mbar. A rotary drive mechanism was used to rotate the substrate holder to obtain good uniformity of the films. The as-deposited films were subsequently annealed in the temperature range 673–973 K in the presence of oxygen ambient (5×10^{-2} mbar) for 2 h to enhance the homogeneity, structural stability and grain size of the films.

XRD measurements were carried out using a computerized X-ray diffractometer, (Siefert model 3003 TT) equipped with a $CuK_{\alpha1}$ radiation (λ=0.15406 nm) source filtered by Ni thin film at a scan speed of 0.03°/s in the 2θ range 10v–60°. The peak positions were determined precisely using RAYFLEX-Analyze software. The surface morphological characteristics of the films have been studied by SEM apparatus (Carl Zeiss, EVO MA 15).

The electrochemical measurements such as CV and chronopotentiometry (CP) were performed by designing aqueous electrochemical cells to understand the fast transport kinetics of the Li ions in $LiMn_2O_4$ thin film positive electrode. The conventional aqueous cell design used in the present study consists of a three-electrode (Pt/saturated Li_2SO_4/$LiMn_2O_4$) cell, which were electrochemically suffused in saturated Li_2SO_4 aqueous electrolyte media. The rf-sputtered LMOFs coated on metallized silicon substrate were employed as working electrode (cathode). A platinum counter electrode (anode), which acts as a reversible source and sink of lithium (conducting) ions, and a commercial calomel reference (Hg/Hg^+) electrode, by which the

electrochemical analysis was calibrated in the presence of a saturated Li_2SO_4 aqueous solution as electrolyte, were employed. An electrochemical analyzer (model CHI 608C; CH Instruments Inc., USA) was used for the aqueous cell measurements and is operated in the cut-off voltage between 0.0 and 1.2 V.

Results and discussion

Structural analysis

Figure 1 shows the XRD patterns of $LiMn_2O_4$ films deposited on metallized silicon substrates maintained at 523 K followed by annealing at various temperatures. All the diffraction peaks can be indexed using the spinel cubic structure (*Fd3m* space group) without phase impurities. The films deposited at a substrate temperature of 523 K exhibited XRD pattern (Fig. 1a) showing the weak intense (111) Bragg line of $LiMn_2O_4$ along with noise and with less predominant Au surface reflection located at 2θ=44.4°. As, all the XRD measurements were carried out with a scan rate of 0.03°/s in diffraction angle (2θ) range 15–60° silicon peak cannot be observed. The Ti layer thickness is very low (0.03 μm) relative to the thickness of Au layer (0.3 μm), and hence the XRD measurements displayed only Au deflections along with characteristic $LiMn_2O_4$ peaks.

The nature of this film may be because of low energy exchange between the sputter atoms and substrate surface. The onset of crystallization was observed for the films subsequently annealed at 673 K after deposition. The degree of crystallization in the films is gradually enhanced with the increase of T_a. The films annealed at T_a>673 K exhibited characteristic peaks corresponding to (111), (311), (222) and (400) lines, in which the (111) orientation was predominant for the cubic *Fd3m* symmetry [23]. The observed XRD peaks became sharper with gradual increase of the annealing temperature up to 973 K. As T_a increases, the rearrangement of Li, Mn and oxygen atoms takes place and leads to the formation of polycrystalline LMOFs with larger grain size. Also, a slight shift in the 2θ position of (111) orientation is observed with increasing annealing temperature from 673 to 973 K. The corresponding grain sizes were estimated from the Scherrer`s formula and were found to be in the range 165–350 nm.

Figure 2 shows the variation of lattice parameter of LMOFs as a function of the annealing temperature. The cubic lattice parameter increases from 8.183 to 8.234 Å, when the films are heated from 673 to 973 K. The Mn–Mn and Mn–O interatomic distances are also calculated for the annealed films by considering the oxygen positional parameter (u) as 0.265 and are shown in Fig. 3. The Mn–Mn and Mn–O interatomic distances were also observed to be increased from 2.892 and 1.914 Å to 2.910 and 1.926 Å, respectively, with annealing in the same range of temperature. At low temperature, the $LiMn_2O_4$ films exhibit small values of lattice parameter and interatomic distances that are attributed to small grain sizes for which the framework could be under more compressional strain. As the annealing temperature increases, the compressional strain present in the film decreases due to the increase of grain size. These results are in agreement with the results reported previously [24]. Additional impurity phases like Mn_2O_3 were observed and the intensity of (111) peak was reduced for the films annealed at higher temperatures, i.e., T_a> 973 K. This may be due to the decomposition of lithium or oxygen or both from the spinel structure.

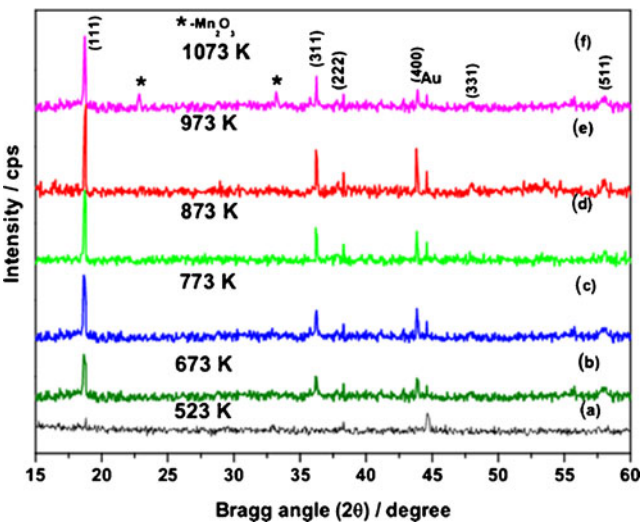

Fig. 1 The X-ray diffraction patterns of $LiMn_2O_4$ thin films grown by rf-magnetron sputtering: **a**)as-deposited at T_s=523 K, forwarded by annealing at temperatures **b** T_a=673, **c** T_a=773, **d** T_a=873 and **e** T_a=973 K

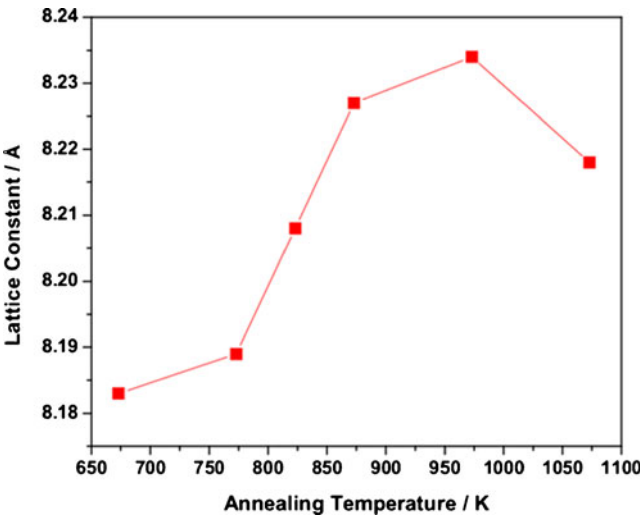

Fig. 2 The cubic lattice parameters of $LiMn_2O_4$ thin films as a function of annealing temperature. Films were deposited at T_s=523 K onto Si/SiO_2 (0.3 μm)/Ti(0.03 μm)/Au(0.3 μm) substrate

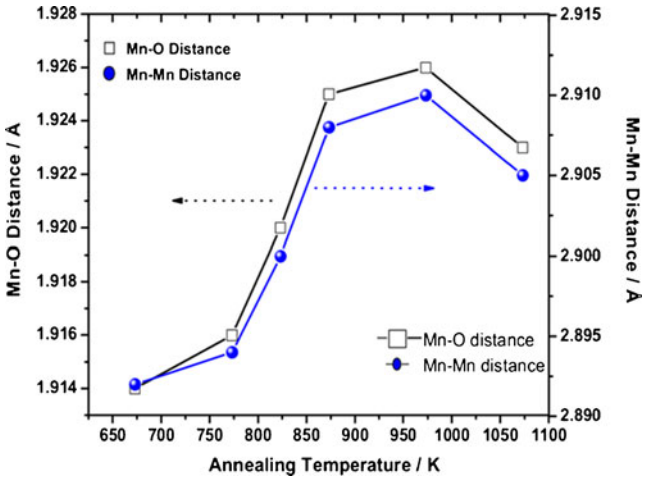

Fig. 3 Variation of Mn–O and Mn–Mn distances with annealing temperature

Surface morphology

Figure 4 displays the SEM images of annealed LMOFs heated at different temperatures. It is observed that the surface morphology of the as-deposited films is almost smooth and no grains are clearly observed (Fig. 4a). A marked improvement in the grain size due to re-crystallization is observed after annealing (Fig. 4a,b). At T_a>700 K, the nucleation occurs and islands are combined and coalesced with each other to form a continuous film with larger grain size. Thus, the changes in the surface features and the improvement in the grain growth are clearly noticed from the SEM images of the films. The film annealed at a temperature of 673 K is composed of plain/smooth surface without predominant grains. Upon increasing the annealing temperature, the grain formation density increases and is clearly noticed from the morphological imaging. The development of surface grains by the adatom mobility is prominent in the films, which induces the variation in the surface interfacial area [17]. The average size of the surface grains for the films annealed at temperature 773 K is about 312 nm and the average grain size of the annealed films at 973 K was found to be 355 nm. Also we notice the uniform distribution of grains and pin-hole free texture of the film without having micro cracks. The estimated average grain size of the annealed films is in close comparison with the respective crystallite sizes that observed from the XRD measurements.

The 3D surface texture of the SEM images for the films annealed at 773 and 973 K were subjected to image processing using the ImageJ software (model 1.44p). Results are shown in Fig. 5a and b. The image processing of the SEM images were carried out in two steps: (1) de-noising using a median filter of radius 9.3 nm (2 pixels) and (2) quantification of grain surface area fraction and surface roughness using the 3D and roughness calculation Java plug-ins. The average area fraction of the surface grains for the films annealed at 773 K is found to be about 55 %, while films annealed at 973 K have an average area fraction of 65 %. It is observed that the area occupied by the surface grains for the films annealed at 773 K is less than the area occupied by the surface grains for the

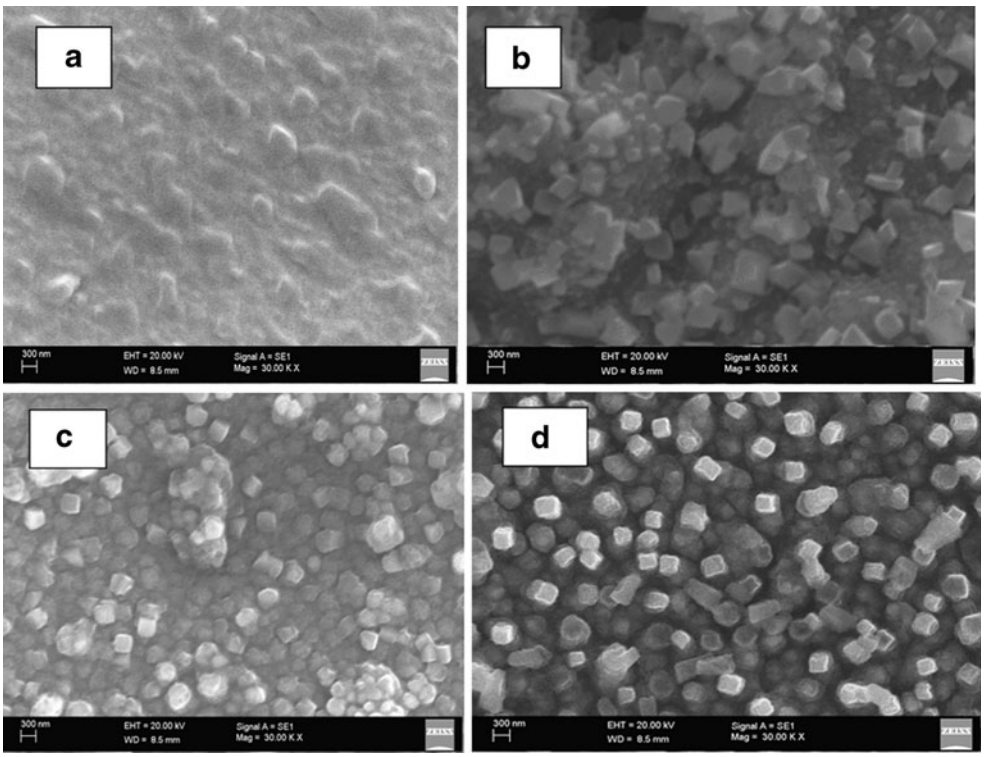

Fig. 4 SEM images of the $LiMn_2O_4$ thin films deposited at **a** T_s=523 K and annealed at **b** T_a=673, **c** T_a=773 and **d** T_a=973 K

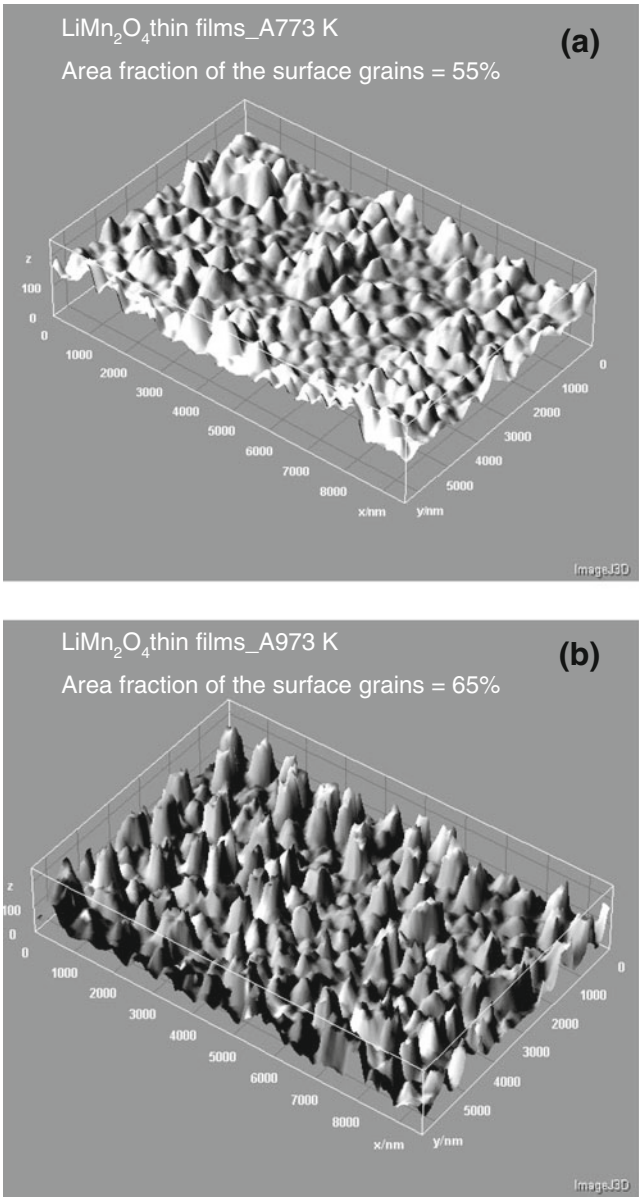

Fig. 5 3D-surface plot of $LiMn_2O_4$ thin films annealed at **a** T_a=773 and **b** T_a=973 K

films annealed at 973 K. This new type of image mapping patterns displaying the development of surface grains in size, which leads to enhancement of surface interfacial area of the $LiMn_2O_4$ films. The surface analysis from the ImageJ software illustrating that the surface roughness of the films was also increasing as a function of annealing temperature. The estimated grain size, grain surface area and the roughness were tabulated in Table 1 for the films annealed at 773 and 973 K. The root mean square (RMS) roughness and arithmetic mean (AM) roughness were observed to be increased in accordance with the annealing temperature. These observations show that such increase of the surface roughness could be favorable for ion insertion because the increase of the interface between the electrode with the electrolyte. The flux of Li ions may increase by the increase of surface area and surface roughness [25]. Hence, the increase in the surface area of the films with high temperature annealing processing could have a positive effect on the electrochemical features. Moreover, the films annealed at 973 K shows well adherent, crystallized, ordered distribution of cubic shaped surface grains with increased surface interfacial area. As shown in the next section, this type of film integrity is favorable for electrochemical testing, especially in terms of charge-transfer capability of the rf-magnetron sputtered LMOFs.

Electrochemical properties

Figure 6a and b shows the cyclic voltammograms recorded at a scan rate of 0.5 mV s^{-1} of the $LiMn_2O_4$ films annealed at (Fig. 6a) 773 and (Fig. 6b) 973 K. Both the plots show two sets of well-separated redox peaks, which correspond to the existence of the two-phase domains of the Li–Mn–O system. In particular, the films annealed at 973 K shows well-resolved redox peaks with a strong current intensity. The peaks located at 0.821 and 0.956 V during cathodic scan (oxidation) correspond to the Li ion deintercalation from the $LiMn_2O_4$ host matrix to form λ-MnO_2, while the peaks located at 0.802 and 0.655 V during anodic scan (reduction) correspond to Li ion intercalation into λ-MnO_2 to form $LiMn_2O_4$. These redox peak potentials are in good agreement with the occurrence of the voltage plateaus observed in the plot of cell voltage vs. discharge capacity (insets of Fig. 6a,b). This is the characteristic property of the spinel $LiMn_2O_4$, for which the insertion–extraction processes of Li^+ ions occur as two-phase reactions involving three cubic phases [26]. The first oxidation peak at 0.821 V is attributed to the removal of lithium ions from half of the tetrahedral sites, whereas the second oxidation peak at 0.956 V is due to the extraction of Li ions from the remaining tetrahedral sites.

The Li^+ ion chemical diffusion coefficient (D_{Li}) in film electrodes has been calculated from data extracted from slow-scan cyclic voltammetry (SSCV) experiments for the $Pt/Li_2SO_4/LiMn_2O_4$ electrochemical cells. The average chemical diffusion coefficient of Li^+ ions, D_{Li}, is given by the following equation [27]

$$i_p = kAn^{3/2}C_0{D_{Li}}^{1/2}v^{1/2}, \quad (1)$$

where i_p is the peak current in the SSCV plot, k=2.69×10^5 is a constant, A is the active surface area of the electrode, n is the number of electrons involved in the reaction, C_0 is the Li^+ concentration in the electrode and v is the sweep rate.

Figure 7 shows the variation of D_{Li} with T_a. According to Eq. 1, the calculated diffusion coefficient for the $LiMn_2O_4$ film annealed at 973 K is about 1.2×10^{-13} cm^2 s^{-1}. Efthekari [28] calculated the diffusion coefficient of the thin films

Table 1 Surface morphological parameters of the $LiMn_2O_4$ films annealed at 773 and 973 K analyzed from ImageJ 1.44p software

Annealed temperature (K)	Grain size (nm)	Area fraction of the grain distribution (%)	Surface roughness	
			RMS (nm)	AM (nm)
773	312	55	97	86
973	355	65	162	156

in presence of aqueous electrolyte and is observed to be around 2×10^{-11} cm^2 s^{-1}. As it is expected, the plot (Fig. 7) demonstrates that for films annealed at higher temperatures are found to have higher Li^+ ion chemical diffusion coefficients leading to greater electrochemical activity. This is due to the improvement in the crystallinity of the grains, the high active surface area of the grains and the surface roughness by annealing. Also, annealing at higher temperatures may increase the adatom mobility and hence the grain size of the films resulting better electrochemical performance.

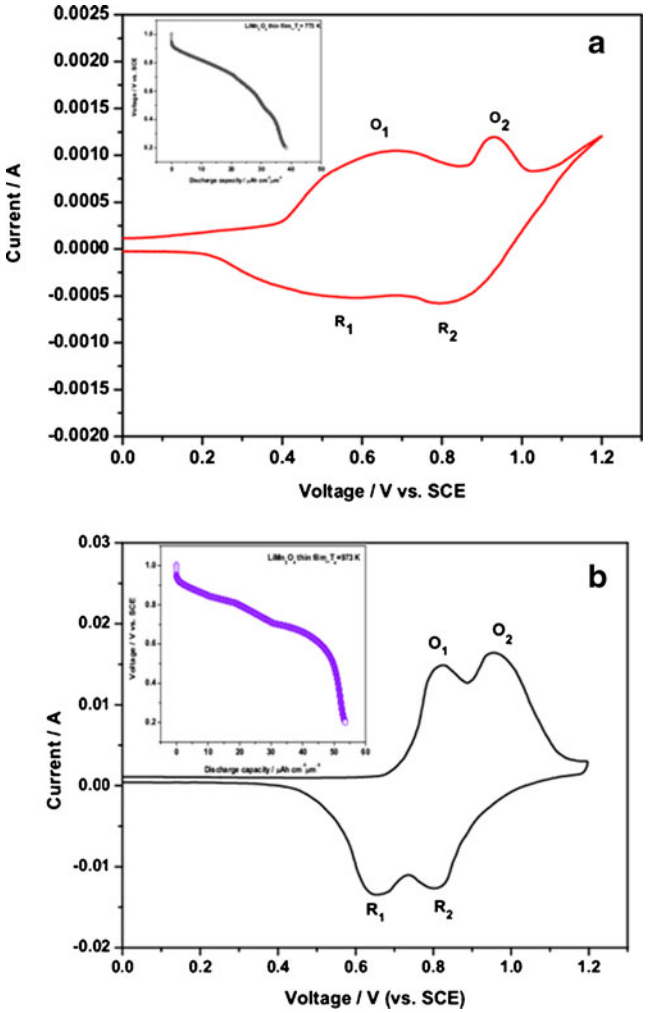

Fig. 6 The cyclic voltammogram and the corresponding specific discharge capacity curve (*inset*) of the $LiMn_2O_4$ film annealed at **a** T_a =773 K and **b** T_a =973 K

Figure 8 shows the discharge profiles of cells with LMOFs annealed at different temperatures. The discharge curves for the as-deposited and films annealed at T_a<673 K display monotonous decay without formation of plateau because of the amorphous nature of the films. The short-range order does not allow us to distinguish between cubic phases. For such films, the estimated discharge capacities are also observed to be very low. Data recorded at the first cycle show that the discharge capacity is 36.6, 38.3, 43.5 and 53.5 μA h cm^{-2} μm^{-1} for the films annealed at 673, 773, 873 and 973 K, respectively. It is clearly seen that the discharge curve of the film annealed at 973 K have two distinct voltage plateaus, which correspond to the reduction process observed in CV experiments. According to previous reports, the upper plateau region represents a two-phase equilibrium between λ-MnO_2 and $Li_{0.5}Mn_2O_4$, whereas the second plateau represents phase equilibrium between $Li_{0.5}Mn_2O_4$ and $LiMn_2O_4$ [29].

Figure 9 shows the graph of the specific discharge capacity vs. cycle number as a function of the annealing temperature. The cyclic retention as a function of annealing temperature is shown in Fig. 10. After 20 cycles, the samples exhibited the discharge capacity of 30.6, 11.0, 8.8 and 8.1 μA h cm^{-2} μm^{-1} and the cyclic retention is 57 %, 25 %, 23 % and 22 %, respectively. The platinum counter electrode could not act as a perfect reversible source and sink of lithium ions and may one of the reasons for the poor cyclic retention of the Pt/Li_2SO_4/$LiMn_2O_4$ cells [30].

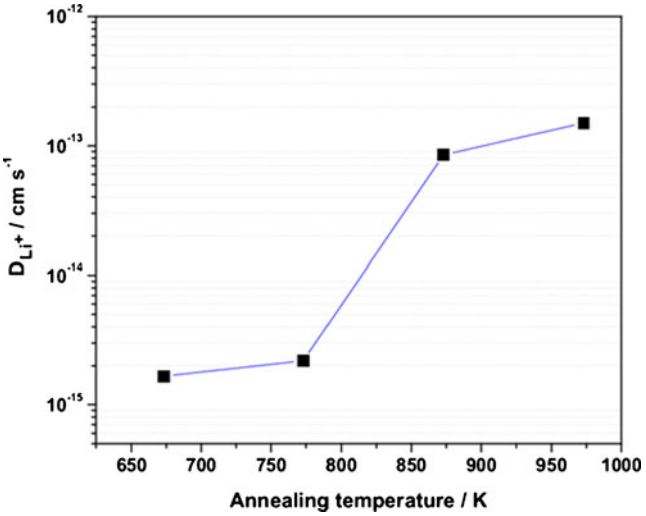

Fig. 7 The chemical diffusion coefficients (D_{Li}) of $LiMn_2O_4$ thin films annealed at different temperatures

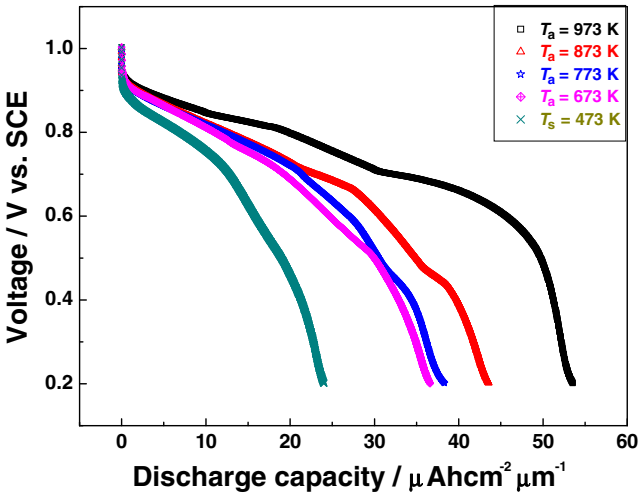

Fig. 8 Initial discharge capacity curves of the $LiMn_2O_4$ thin films annealed at different temperatures

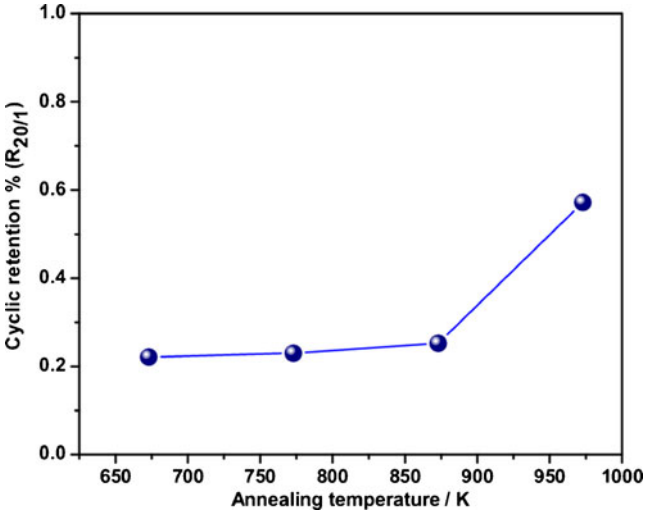

Fig. 10 Discharge cyclic retention of the $LiMn_2O_4$ thin films with different annealing temperatures

Finally, it is noticed that the films annealed at 673 K has a lower discharge capacity upon electrochemical cycles, which is due to poor crystallinity as a result of the formation of amorphous structure. The films annealed at 773 K have insignificant enhancement in the initial discharge capacity and its structural stability is also very poor, whereas the films annealed at 873 K has shown better cyclability, which is attributed to its good crystallinity. Further improvement in the cyclic retention with good discharge capacity is noticed for the films annealed at 973 K because the predominant (111)/(311) orientations is advantageous for the Li^+ extraction/insertion from/to the spinel lattice. Finally, we remark that the large extent of agglomeration of particles and the formation of the cracks in the film annealed at T_a>1,000 K reduced the electrochemical performance of the films. From the above discussion, the post-annealing process of rf-magnetron sputtered $LiMn_2O_4$ films prepared on metallized silicon substrates at elevated temperatures under controlled oxygen environment leads to an increase of surface interfacial area, which results in better cycling performance.

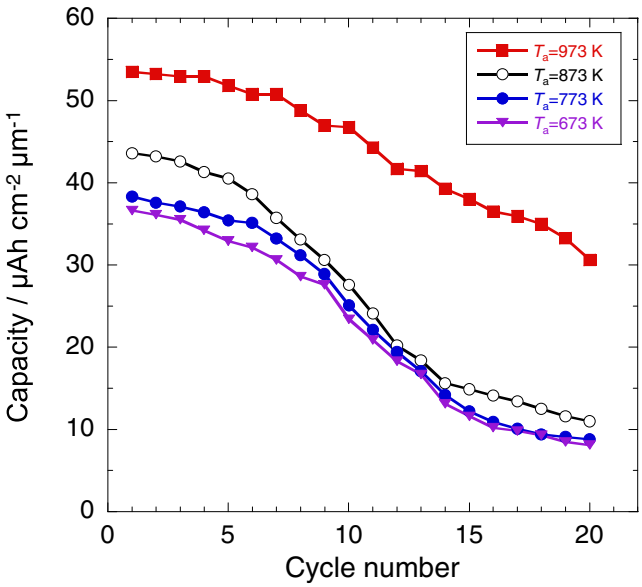

Fig. 9 Cycling performance of the $LiMn_2O_4$ thin films with different annealing temperatures

Conclusion

$LiMn_2O_4$ films with good adhesion have been fabricated on metallized silicon substrate by rf-magnetron sputtering technique. The influence of annealing temperature on the microstructural and electrochemical properties of $LiMn_2O_4$ films was studied. The degree of crystallization of the films gradually increased with the increase of annealing temperature. The films annealed at higher temperature exhibited characteristic peaks corresponding to (111), (311), (222) and (400) orientations of the spinel structure with the cubic *Fd3m* symmetry. The lattice parameter increased from 8.183 to 8.234 Å and the Mn–Mn and Mn–O interatomic distances were also observed to be increased. Typical changes in surface morphology of the films were observed by SEM. The average area fraction of the surface grains for the films annealed at 973 K was found to be about 65 %. The surface analysis illustrated that the surface roughness of the films was also increasing as a function of annealing temperature. The slow sweep CV (and CP) measurements were carried out by designing $Pt/Li_2SO_4/LiMn_2O_4$ aqueous cell. The electrochemical features show two very active redox peaks that are characteristic of the extraction–insertion of Li^+ ions from/into the spinel framework. The $Pt/LiMn_2O_4$ electrochemical cell with $LiMn_2O_4$ film annealed at 973 K exhibited an initial discharge capacity of about 53.5 μA h cm^{-2} μm^{-1}. The calculated Li^+ ion chemical

diffusion coefficient is about 1.2×10^{-13} cm^2 s^{-1}. The above results also show that the replacement of non-aqueous media by aqueous media makes an interesting test for the preliminary study of cathode materials in thin film form.

Acknowledgements Dr. O.M. Hussain thanks the DRDO, Hyderabad, India, for providing financial support to this study.

References

1. Thackeray MM, David WIF, Bruce PG, Goodenough JB (1983) Mater Res Bull 18:461–472
2. Thackeray MM (1997) Prog Solid State Chem 25:1–71
3. Thackeray MM (1995) J Electrochem Soc 142:2558–2563
4. Manjunatha H, Mahesh KC, Suresh GS, Venkatesha TV (2011) Electrochim Acta 56:1439–1446
5. Amatucci G, Pasquier AD, Blyr A, Zheng T, Tarascon JM (1999) Electrochim Acta 45:255–271
6. Mishra SK, Ceder G (1999) Phys Rev B 59:6120–6130
7. Chiang YM, Wang H, Jang YI (2001) Chem Mater 13:53–63
8. Fergus JW (2010) J Power Sources 195:939–954
9. Hussain OM, Harikrishna K, Kalaivani V, Julien CM (2007) Ionics 13:455–459
10. Kalai-Vani V, Hussain OM (2007) Ionics 13:473–477
11. Shih FY, Fung KZ (2006) J Power Sources 159:179–185
12. Shui JL, Jiang GS, Xie S, Chen CH (2004) Electrochim Acta 49:2209–2213
13. Rho YH, Dokko K, Kanamura K (2006) J Power Sources 157:471–476
14. Chen CC, Chiu KF, Lin KM, Lin HC (2009) Thin Solid Films 517:4192–4195
15. Xie J, Tanaka T, Imanishi N, Matsumura T, Hirano A, Takeda Y, Yamamoto O (2008) J Power Sources 180:576–581
16. Komaba S, Kumagai N, Baba M, Miura F, Fujita N, Groult H, Devilliers D, Kaplan B (2000) J Appl Electrochem 30:1179–1182
17. Kim WS (2004) J Power Sources 134:103–109
18. Beck F, Ruetschi P (2000) Electrochim Acta 45:2467–2482
19. Ruffo R, La Mantia F, Wessells C, Huggins RA, Cui Y (2011) Solid State Ionics 192:289–292
20. Li W, Dahn JR, Wainwright DS (1994) Science 264:1115–1118
21. Park M, Zhang X, Chung M, Less GB, Sastry AM (2010) J Power Sources 195:7904–7929
22. Eftekhari A (2001) Electrochim Acta 47:495–499
23. Shih FY, Fung KZ (2007) J Alloys Compd 430:320–329
24. Shinshu F, Kaida S, Nagayama M, Nitta Y (1997) J Power Sources 68:609–612
25. Simmen F, Lippert T, Novák P, Neuenschwander B, Döbeli M, Mallepell M, Wokaun A (2008) Appl Phys A 93:711–716
26. Okubo M, Mizuno Y, Yamada H, Kim J, Hosono E, Zhou H, Kudo T, Honma I (2010) ACS Nano 4:741–752
27. Wang GJ, Qu QT, Wang B, Shi Y, Tian S, Wu YP, Holze R (2009) Electrochim Acta 54:1199–1203
28. Efthekari A (2001) Electrochim Acta 47:495–499
29. Li W, Dahn JR (1995) J Electrochem Soc 142:1742–1746
30. Wang GJ, Qu QT, Wang B, Shi Y, Tian S, Wu YP, Holze R (2009) Electrochim Acta 54:1199–1203